energies

MDPI

Review

Carbon and Electron Recovery in Integrated Biohydrogen Systems: A Critical Review of Dark Fermentation, Photo-Fermentation, and Microbial Electrolysis Cells

Ravi Shankar Yadav and Ju-Hyeong Jung *

Department of Environmental Engineering, Kunsan National University, Gunsan 54150, Republic of Korea
* Correspondence: jhjung@kunsan.ac.kr; Tel.: +82-63-469-1873

Abstract

Hydrogen is increasingly recognized as a key energy carrier for decarbonizing hard-to-electrify sectors, yet more than 95% of current global production remains fossil-derived. Biological hydrogen (biohydrogen) produced by dark fermentation (DF), photo-fermentation (PF), or microbial electrolysis cells (MEC) offers the dual advantage of valorizing organic wastes while delivering low-carbon H_2; however, none of these standalone technologies mobilizes more than 25–33% (DF), 40–70% (PF), or 40–60% (MEC) of feedstock organic carbon through H_2-producing oxidation pathways. Most existing reviews compare these pathways on hydrogen yield alone, a metric that conceals where the majority of feedstock carbon and electrons are actually lost and obscures the quantitative rationale for system integration. This review reframes the comparison around carbon and electron flow, explicitly tracking how much input carbon is mobilized through H_2-producing oxidation pathways, how much is retained in volatile fatty acids (VFAs), biomass, or unlinked CO_2, and what happens to the associated electrons. Stoichiometric, mechanistic, and reactor-level evidence is synthesized to show that DF channels only 25–33% of input organic carbon through H_2-yielding decarboxylation on real heterogeneous substrates, with 40–60% retained as residual VFAs and unhydrolyzed solids; PF can recover 60–80% of VFA carbon but is constrained by photon economics and nitrogenase sensitivity; and MEC achieves >85% COD removal only when coupled to an upstream acidogenic stage. Two-stage (DF–PF, DF–MEC) and three-stage (DF–PF–MEC, DF–MEC–AD) configurations are critically evaluated, with theoretical yields separated from experimentally demonstrated performance on real wastes and hidden energy inputs (pretreatment, inter-stage transfer, gas separation, and compression) explicitly accounted for. DF–MEC coupling is identified as the most near-term tractable configuration, achieving 55–70% H_2-pathway carbon mobilization and 80–92% COD removal at an electrical input of 0.9–1.5 kWh/m^3 H_2, with levelized hydrogen costs of US$3–5.5/kg under favorable waste-tipping-fee conditions. Multi-stage systems push carbon recovery above 70% but carry unresolved capital, methanogenesis control, and scale-up penalties. This review closes by proposing a standardized ten-descriptor reporting framework including H_2-pathway carbon mobilization (%), cathodic hydrogen recovery (rCAT), net energy recovery (NEB), and LCA carbon intensity under both attributional and consequential boundaries, and demonstrates its backward compatibility by retrospective application to seven studies already in the literature. Research priorities tractable on a 5–10 year horizon are identified, centered on methanogen suppression at pilot scale, real-waste MEC performance, and renewable-electricity coupling.

Check for updates

Academic Editor: Alberto Pettinau

Received: 23 May 2026
Revised: 23 June 2026
Accepted: 28 June 2026
Published: 2 July 2026

Copyright: © 2026 by the authors. Licensee MDPI, Basel, Switzerland. This article is an open access article distributed under the terms and conditions of the Creative Commons Attribution (CC BY) license.

Keywords: biohydrogen; system integration; electron balance; life-cycle assessment; techno-economic analysis

1. Introduction

The global hydrogen sector, therefore, occupies a structurally contradictory position. Hydrogen is widely promoted as a low-carbon energy carrier, while the overwhelming majority of its production remains fossil-derived and carbon-intensive. It is widely cited as essential for decarbonizing hard-to-electrify sectors, long-haul transport, ammonia synthesis, primary steel, and high-temperature industrial heat, yet roughly 95% of the ~95 Mt of H_2 produced annually is still derived from steam methane reforming (SMR) or coal gasification, contributing on the order of 900 Mt CO_2/y [1,2]. Replacing this fossil base with "green" hydrogen is therefore not a niche objective but a precondition for several decarbonization pathways. Water electrolysis powered by renewable electricity is the dominant technology being scaled, but it is electricity-intensive (≈50–55 kWh/kg H_2) and competes directly with electrification of grids and transport for the same renewable kilowatt-hour [2].

Biological hydrogen (biohydrogen) occupies a different and complementary niche. Rather than splitting purified water with renewable electricity, biological systems oxidize reduced carbon already present in organic wastes and residues, releasing electrons that can be captured as H_2 either fermentatively, photochemically, or electrochemically [3,4]. The feedstock, therefore, performs double duty as both an electron donor and a waste-management problem to be solved. Three biological hydrogen routes have received sustained attention: (i) dark fermentation (DF), in which mixed or defined anaerobes ferment carbohydrates to H_2, CO_2 and volatile fatty acids (VFAs); (ii) photo-fermentation (PF), in which purple non-sulfur bacteria use light energy to drive nitrogenase-mediated proton reduction from VFAs and other reduced substrates; and (iii) microbial electrolysis cells (MEC), bioelectrochemical reactors in which exoelectrogens oxidize organics at an anode and an applied voltage of 0.2–0.8 V drives proton reduction to H_2 at a cathode [5].

Each of these technologies has been reviewed individually, often extensively [6]. Most such reviews compare technologies on the basis of hydrogen yield, expressed as mol H_2 per mol hexose or mL H_2 per g volatile solids. While useful, that metric is also misleading; it obscures the fact that the dominant fate of feedstock carbon in standalone biological hydrogen systems is not H_2 at all. In DF, the thermodynamic ceiling of 4 mol H_2/mol glucose via the acetate pathway corresponds to only ~33% of the carbon being released as CO_2, with the remaining 67% retained as VFAs that are typically discarded as a waste stream [3,7]. The headline yield metric, therefore, says nothing about what happens to the largest carbon pool. Similar accounting blind spots affect comparisons of PF (high theoretical yield from acetate but very low volumetric productivity) and MEC (high COD removal but only on an electron-donor stream that DF must produce first).

A more informative organizing principle is carbon and electron flow: of the carbon and electrons entering the reactor train, what fraction emerges as H_2, what fraction is irrecoverably lost as CO_2, and what fraction remains in residual organics or biomass? Framed this way, the case for integration is no longer a vague appeal to "synergy" but a quantitative one. The VFAs that DF cannot oxidize further are an ideal anode substrate for MEC; the acetate fraction of DF effluent is an ideal substrate for nitrogenase-mediated PF; the residual COD that escapes a single MEC pass can be polished by anaerobic digestion (AD) into methane. Each integration step is, in principle, a step toward closing the carbon and electron loop on the same [8] feedstock.

Several recent reviews have begun to evaluate integrated configurations. Most, however, either focus on a single integration pair (typically DF–PF) or treat the integration question primarily as one of process engineering rather than electron accounting. Comparative tables in these reviews tend to mix theoretical maxima, lab-scale demonstrations on synthetic substrates, and pilot data on real wastes without distinguishing among them, making the resulting performance ranges difficult to interpret. Reporting conventions also vary widely: yields are normalized to hexose, to total solids, to volatile solids, or to chemical oxygen demand (COD), often without enough information to convert between them [6,9–11].

Scope and Novelty of This Review

Rather than presenting itself as the first review of integrated biohydrogen systems, this article defines its contribution more specifically as a critical synthesis centered on carbon and electron recovery. The review provides a carbon- and electron-flow-based evaluation of dark fermentation (DF), photo-fermentation (PF), microbial electrolysis cells (MECs), and their integrated configurations. Three specific aspects distinguish this review. First, theoretical performance is separated from experimentally demonstrated performance in the comparative analysis, while synthetic-substrate studies are distinguished from real-waste applications wherever sufficient data are available. Second, particular attention is given to DF–MEC coupling because this configuration offers a comparatively practical balance between hydrogen recovery, residual COD removal, energy input, methanogenesis control, and scale-up potential. Third, a standardized minimum reporting framework for carbon and electron recovery is proposed to improve comparability among future integrated-biohydrogen studies and to support more defensible techno-economic and life-cycle assessments. Overall, this review does not treat integration as an inherently superior solution; instead, it critically examines where carbon and electrons are recovered, where losses occur, and which reported performance values are sufficiently supported by experimental evidence.

2. Standalone Biohydrogen Pathways

To establish the rationale for system integration, the first step is to identify where carbon and electrons are lost within each standalone technology. Accordingly, this section examines dark fermentation, photo-fermentation, and microbial electrolysis cells individually (Figure 1), followed by a comparative assessment of their carbon recovery performance in Table 1.

2.1. Dark Fermentation

Dark fermentation is the most mature of the three biological hydrogen technologies, with multiple pilot demonstrations and a Technology Readiness Level (TRL) of approximately 6, indicating technology demonstrated in a relevant environment or pilot scale setting [7,12]. Glucose is catabolized through glycolysis to pyruvate, which is oxidatively decarboxylated to acetyl-CoA by pyruvate: ferredoxin oxidoreductase (PFOR) in *clostridia*, releasing CO_2 and reducing ferredoxin. Reduced ferredoxin is re-oxidized by [FeFe]-hydrogenases, producing H_2. In facultative anaerobes such as *Enterobacter*, the formate hydrogen lyase (FHL) complex provides an alternative route, oxidizing formate to $H_2 + CO_2$ [3,13].

The much-cited stoichiometric ceiling of 4 mol H_2/mol glucose via the acetate pathway is rarely approached in practice. Three observations matter for carbon accounting. First, the acetate pathway itself releases two of the six carbon atoms as CO_2 and retains four as acetate; only the H_2 leaves the system as recovered energy, while the acetate carbon

remains in the effluent. Second, mixed cultures shift toward butyrate (yielding 2 mol H_2/mol glucose), ethanol (0 mol H_2 in pure ethanol fermentation), lactate (0 mol H_2), and propionate (which actually consumes H_2) under thermodynamic stress, low pH, or elevated H_2 partial pressure [7,14]. Third, on real lignocellulosic or food-waste substrates, hydrolysis is typically rate-limiting and a significant fraction of substrate carbon ends up in microbial biomass rather than fermentation products. Practical yields on real wastes therefore cluster between 1.0 and 2.5 mol H_2/mol glucose-equivalent [15].

Translated to a carbon balance, standalone DF on real organic wastes typically converts 25–33% of input organic carbon to H_2-equivalent (i.e., carbon released as CO_2 in the H_2-yielding decarboxylation), 40–60% remains in the effluent as Volatile fatty acids (VFAs), alcohols, and unhydrolyzed solids, and the balance is bound in biomass. The 40–60% residual carbon stream is simultaneously the principal motivation for integration, as it represents recoverable energy and electrons, and the principal economic problem of standalone DF, because it constitutes a high-strength wastewater that must be treated.

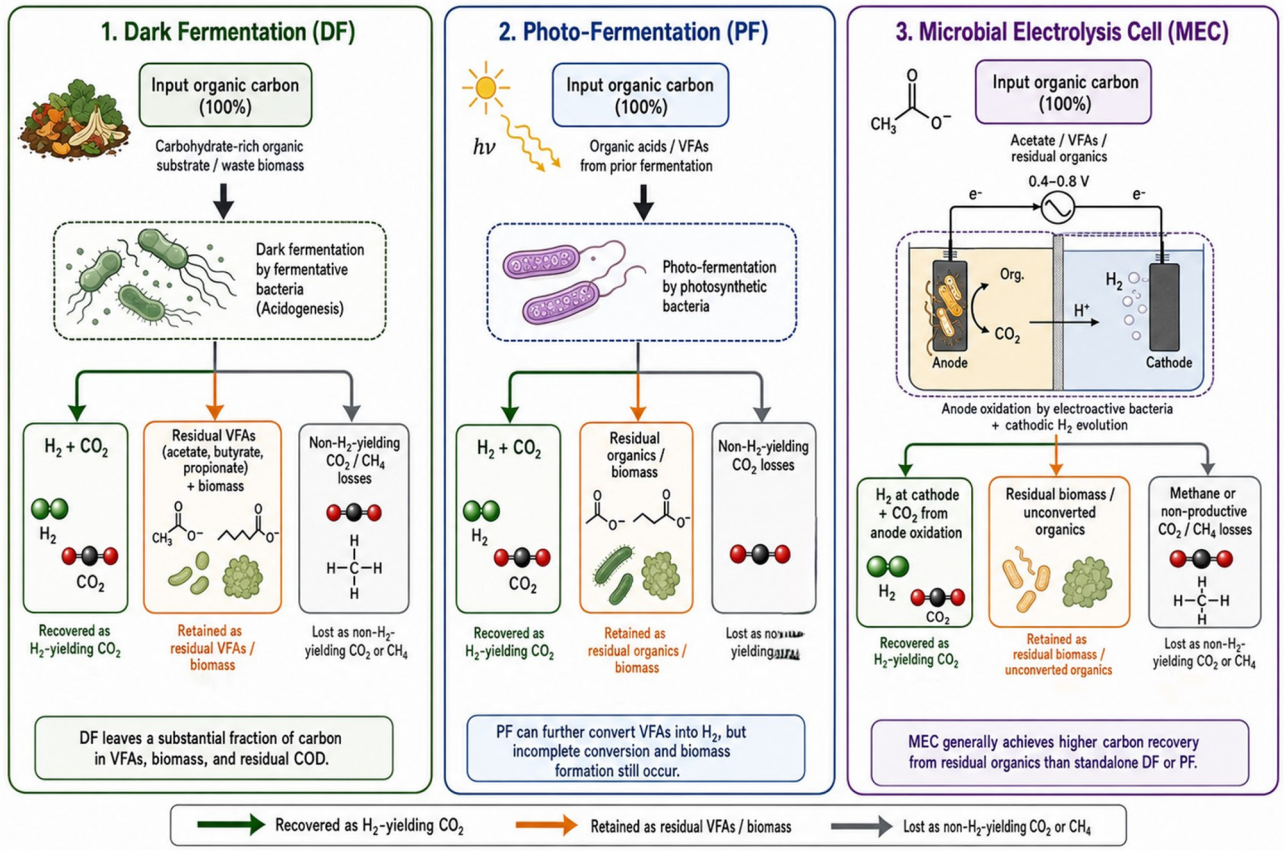


Figure 1. Carbon partitioning in standalone biohydrogen technologies. Schematic representation of the fate of input organic carbon during dark fermentation (DF), photo-fermentation (PF), and microbial electrolysis cell (MEC) operation. Numerical ranges shown reflect typical values reported for real-waste operation in the cited literature (Table 1) and are not single-source measurements.

2.2. Photo-Fermentation

Photo-fermentation by purple non-sulfur (PNS) bacteria, chiefly *Rhodobacter sphaeroides*, *Rhodopseudomonas palustris*, and *Rhodospirillum rubrum*, uses light energy to drive nitrogenase, which under nitrogen-limited conditions reduces protons to H_2 rather than fixing N_2 [16–18]. The acetate-to-H_2 stoichiometry, $CH_2COOH + 2H_2O \rightarrow 4H_2 + 2CO_2$, is endergonic ($\Delta G^\circ \approx +104$ kJ/mol) and requires light input; combined with DF acetate output, the two-stage theoretical maximum reaches 12 mol H_2/mol glucose [3,19].

Two practical constraints undermine this attractive theoretical picture. The first is photon economics. Effective volumetric H_2 productivities of PF are typically 0.5–3 mmol/L/h, an order of magnitude below DF, because dense bacterial suspensions self-shade and outdoor light conversion efficiencies rarely exceed 3–5% even in optimized flat-panel or fibre-illuminated bioreactors [16,20]. The second is sensitivity to feedstock chemistry. Nitrogenase is strongly inhibited by ammonium (typically above ~2 mM NH_4^+) and requires C/N ratios above ~25–40 for efficient H_2 production. DF effluents from protein-rich wastes (food waste, dairy effluent, slaughterhouse wastewater) often violate both criteria, requiring dilution, ammonia stripping, or membrane conditioning before being fed to a PF reactor [21,22].

From a carbon-flow perspective, PF can, in principle, recover 60–80% of VFA carbon as H_2, which is much higher than DF on hexoses. Whether this advantage translates to overall system performance depends entirely on whether enough VFA can actually be processed within reasonable photobioreactor volumes, a constraint examined quantitatively in Section 3.2.

2.3. Microbial Electrolysis Cells

Microbial electrolysis cells were proposed as a modification of microbial fuel cells in which a small applied voltage shifts the cathodic half-reaction from oxygen reduction to proton reduction, allowing the electrons captured by exoelectrogens to be recovered as H_2 [23,24]. The dominant exoelectrogens are members of the *Geobacter* genus, which transfer electrons to the anode through outer-membrane c-type cytochromes and conductive pili; Shewanella and mixed-community exoelectrogens are also relevant, particularly in real-waste reactors [4,25,26].

For acetate, the standard half-cell potentials give a thermodynamic minimum applied voltage of approximately 0.14 V; in practice, 0.2–0.8 V is required to overcome ohmic losses, biofilm overpotential, and pH gradients between anode and cathode chambers [4,27]. Two performance descriptors are central. Coulombic efficiency (CE), the fraction of substrate electrons recovered in the external circuit, ranges from 60–90% on acetate but is substantially lower on complex substrates due to fermentative side-reactions and methanogenesis [5,28]. Cathodic hydrogen recovery (rcat), the fraction of cathodic electrons appearing as H_2, exceeds 90% with efficient cathodes but degrades when methanogen colonies the cathode and re-consume H_2. Overall H_2 recovery $rH_2 = CE \times rcat$ is therefore the appropriate system-level descriptor; reported values on synthetic acetate cluster at 55–85% but drop to 30–60% on real fermentation effluents [13].

MECs are unique among the three technologies in that their input is electrons (and protons), not photons or chemical-free energy alone. This makes them naturally complementary to DF: DF supplies the VFA-rich electron donor, MEC supplies the electrochemical pull that DF cannot generate from the same molecules. It also means that the carbon footprint of MEC hydrogen is sensitive to the carbon intensity of the input electricity, a point sometimes glossed over in techno-economic analysis (TEA) studies (see Section 6).

2.4. Comparative Carbon Efficiency

Table 1 summarises the three pathways and their integrated configurations on a common set of descriptors. Several points warrant emphasis. The "H_2-pathway Carbon mobilization" row is computed as the fraction of input organic carbon released as CO_2 in H_2-yielding oxidation steps (i.e., carbon whose corresponding electrons are recovered as H_2); it is not the same as COD removal. Standalone DF and standalone MEC are essentially complementary on this metric. DF recovers 25–33% from hexoses, MEC recovers 40–60% from VFA-like substrates that DF cannot further oxidize. PF achieves the highest single-

stage H_2-pathway Carbon mobilization recovery on suitable VFA streams, but pays for it in volumetric productivity. Only the integrated configurations approach 65–80% H_2-pathway Carbon mobilization recovery, and only at the cost of additional reactor volume and process control complexity [29].

Table 1. Comparative summary of standalone and integrated biohydrogen production pathways.

Parameter.	DF	PF	MEC	DF–PF	DF–MEC	DF–PF–MEC/ DF–MEC–AD	Key References
Theoretical H_2 yield	4 mol/mol glucose	8 mol/mol HAc	Limited by e^- supply	12 mol/mol glucose	~10 mol/mol glucose	12 mol/mol glucose	[3,13]
Practical H_2 yield (real wastes)	1.0–2.5 mol/mol glucose	2–4 mol/mol HAc	0.5–2.5 mol/mol glucose	3–5 mol/mol glucose	4–7 mol/mol glucose	5–9 mol/mol glucose	[12,30,31]
H_2-pathway C mobilization (%) *	25–33	40–70	40–60	40–55	55–70	65–80	[7,10]
COD removal (%)	40–60	60–80	70–95 (synth.); 50–80 (real)	55–70	80–92	85–95	[5,28]
Volumetric H_2 rate (mmol/L/h)	5–15	0.5–3	0.5–10	2–8	3–12	4–15	[16,25]
Coulombic eff. (%) #	n/a	n/a	60–90 (synth); 40–70 (real)	n/a	50–80	50–80	[28,30]
TRL	6–7	3–5	4–5	3–4	3–4	2–3	[1,5]
Dominant residual C	VFAs, biomass	CO_2, biomass	CO_2, residual VFA	Residual HAc, HPr, HBu	CO_2, traces	<5% residual COD	—

* H_2-pathway Carbon mobilization (%) is the fraction of input organic carbon that passes through oxidation reactions directly coupled to H_2 evolution. This metric does not imply carbon atoms are incorporated into H_2 (H_2 contains no carbon); it quantifies how much substrate carbon is 'activated' toward H_2 production through decarboxylation or coupled oxidation steps. Values on real wastes are 30–50% lower than synthetic-substrate benchmarks (Supplementary Table S1, paired analysis across 12 studies). Values are mechanistically distinct from COD removal (see Section 2.4). # Coulombic efficiency (CE) values represent overall system efficiency (electrons recovered as H_2 at cathode relative to theoretical electrons from substrate COD oxidation), following [24]. CE integration window: stable-state operation (>10 HRTs) to end of experiment; start-up phase excluded. Anode-only CE is 5–15 percentage points higher than the overall system CE reported here. HAc = acetic acid; HPr = propionate; HBu = butyrate; VFA = volatile fatty acids; TRL = Technology Readiness Level; n/a = not applicable.

3. Integrated Biohydrogen Systems

We use carbon and electron loop closure in a deliberately restrictive sense: the design objective of minimizing the fraction of input organic carbon (and the associated electrons) that exits the reactor train as anything other than H_2 or biologically captured CO_2. Three caveats follow immediately. First, perfect closure is thermodynamically impossible. CO_2 is the inevitable terminal product of complete substrate oxidation, and 3–10% of substrate carbon is irrecoverably diverted into biomass. Second, "closing the loop" does not by itself imply economic viability; a system can be carbon-efficient and economically unviable, or vice versa. Third, the term as we use it is engineering, not rhetorical: it refers to specific, measurable carbon and electron balances rather than to a generic appeal to circularity [9]. Carbon and electron recovery in integrated biohydrogen systems are demonstrated in Figure 2.

With these caveats, the gap between standalone DF (25–33% C-to-H_2) and integrated three-stage systems (65–80%) represents an improvement of roughly 2.5–3× in H_2 output per unit feedstock, and a corresponding reduction in residual COD that must be separately treated. This is a sufficiently large margin that even imperfect integration yields meaningful gains.

3.1. DF–PF Integration

DF–PF was historically the first integration pair to receive serious attention because the substrate match is mechanistically clean: DF effluent is rich in acetate and butyrate,

both of which are good substrates for PNS bacteria under nitrogen limitation. Reported combined yields range from 4 to 8 mol H_2/mol glucose in lab-scale demonstrations on synthetic substrates and 3–5 mol/mol on real wastes [12,20,21,32,33].

The persistent constraints are physical and chemical, not biological. Physically, PF volumetric productivities (0.5–3 mmol/L/h) are 3–10× lower than DF, so balanced continuous operation requires PF reactor volumes that are correspondingly larger. This penalty is rarely costed transparently in literature. Chemically, ammonium concentrations in DF effluent from protein-containing wastes routinely exceed nitrogenase tolerance, and pH adjustment from DF (pH 5.5–6.0) to PF (pH 6.8–7.5) requires base addition that adds operating cost and salinity. Membrane conditioning (nanofiltration to retain ammonium while passing VFAs) can resolve the chemistry but multiplies capital cost [21]. On balance, DF–PF is mechanistically attractive; however, its practical deployment remains constrained by low photobioreactor productivity, large illuminated surface area requirements, and feed conditioning costs reported in lab and pilot-oriented studies. These constraints partly explain the recent shift in attention toward MEC-based integration.

3.2. DF–MEC Integration

The case for DF–MEC rests on five points, each of which can be evaluated quantitatively. (i) Substrate fit: DF effluents are dominated by acetate, butyrate, and propionate, and *Geobacter*-enriched anode biofilms oxidize acetate and butyrate efficiently (CE 60–85% on acetate, 50–70% on butyrate) [28,34]. (ii) Energy penalty: at applied voltages of 0.4–0.6 V and Faradaic efficiencies typical of pilot MECs, electrical inputs are 0.9–1.5 kWh/m^3 H_2 produced well below the ~5 kWh/m^3 of alkaline water electrolysis on a hydrogen-volume basis [24,30]. (iii) COD removal: pilot and bench scale DF–MEC trains have reported 80–92% COD removal across the integrated system under the specific reaction times or hydraulic retention times (HRT) used in the respective studies; therefore, this range should be interpreted as residence time dependent rather than as fixed process constant [35,36]. (iv) No light dependence: unlike DF–PF, DF–MEC operates 24/7 and is geographically unconstrained. (v) Scale-up trajectory: the 100–1000 L MEC pilots demonstrate that the technology can leave the bench, even if no commercial-scale unit has yet been built [17,28,30,37].

Three challenges deserve specific critical attention because they are routinely underplayed in the optimistic literature. First, methanogenesis is the dominant route by which MEC efficiency degrades on real substrates: hydrogenotrophic methanogens (*Methanobacterium*, *Methanobrevibacter*) consume cathodic H_2, while acetoclastic methanogens (*Methanosaeta*) compete with exoelectrogens for acetate. Reported mitigation strategies, periodic air sparging, low pH operation, 2-bromoethanesulfonate (BES) dosing, and physical exclusion via ion-exchange membranes each carry penalties, and none has yet been demonstrated as a robust long-term solution at pilot scale [34,38]. Second, cathode catalyst cost: although biocathode and stainless-steel mesh cathodes have largely displaced platinum in the recent literature, internal resistance and overpotential rise correspondingly, and reported H_2 recoveries on these cheaper cathodes typically fall to 60–80% under real-effluent conditions [4,39–41]. Third, the "ohmic wall" of MEC scale-up: as electrode area and electrolyte volume grow, internal resistance rises non-linearly and current densities fall, a problem that 3D-printed and stacked cell architectures partially address but do not eliminate [17,25,42].

3.3. Three-Stage and Hybrid Systems

Three-stage configurations (DF–PF–MEC; DF–MEC–AD; DF–MEC–MES) push reported H_2-pathway Carbon mobilization$_2$ conversion above 70% in lab demonstrations. They are conceptually clean: each successive stage targets the carbon and electron pool

that the previous stage cannot reach. In practice, however, the incremental yield from a third stage is typically 15–25% above the two-stage baseline, while capital cost and process control complexity roughly double. The economic case for three-stage systems is currently restricted to high-tipping-fee waste contexts (food waste, slaughterhouse waste, brewery effluent) where waste-treatment revenue offsets capital amortization [9,10,43,44].

DF–MEC–AD is a particularly interesting hybrid because it explicitly chooses total energy recovery (H_2 + CH_4) over H_2 yield maximization, recognizing that the residual COD escaping MEC is most efficiently captured as methane rather than as additional H_2. For waste-treatment applications where the operator is paid per unit COD removed, this is often the most economically rational configuration. It blurs the boundary between "biohydrogen plant" and "advanced anaerobic digester," a blurring that we view as productive rather than problematic [10,35].

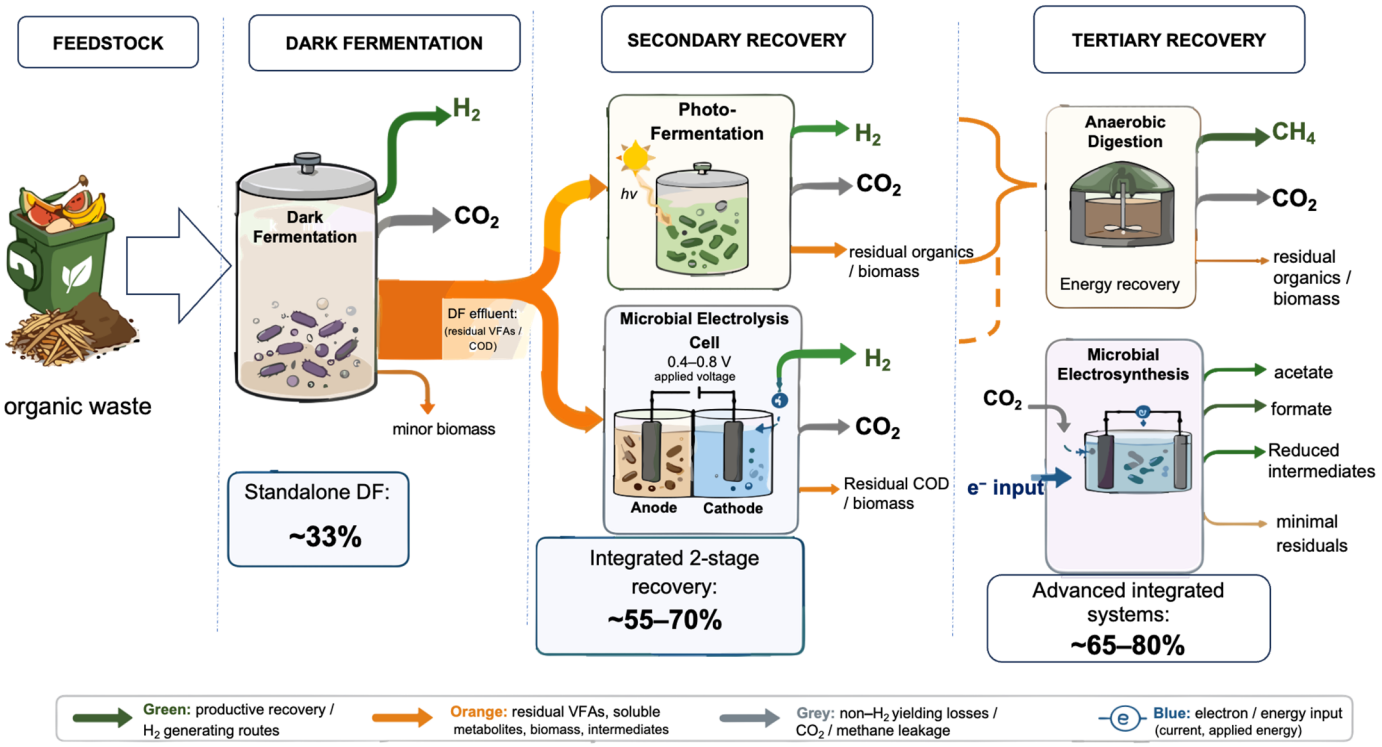


Figure 2. Carbon and electron recovery in integrated biohydrogen configurations. Cumulative carbon to H_2 recovery ranges are midpoint values derived from Tables 1 and 2 and are shown for conceptual comparison.

4. Feedstock Utilization and Resource Efficiency

Three feedstock attributes maximize the performance of integrated biohydrogen trains: (i) high readily fermentable carbohydrate content for DF, (ii) C/N ratio above ~25 and low ammonium for downstream PF, (iii) low concentrations of inhibitors (furans, phenolics, heavy metals, sulfide) for MEC anode biofilms. No real waste stream simultaneously satisfies all three.

4.1. Major Feedstock Categories

Lignocellulosic agricultural residues represent the largest terrestrial organic carbon pool available for bioconversion, with Asia alone generating an estimated 1.3–1.5 Gt/yr of crop residues, dominated by rice straw and wheat straw [45–47]. Their high cellulose/hemicellulose content (50–75% of dry weight) and naturally low N content match

DF–PF chemistry well, but the lignocellulosic matrix is recalcitrant. Pretreatment is unavoidable and contributes both to energy demand and inhibitor formation [11].

Food waste and organic municipal solid waste (OMSW) are at the opposite end of the spectrum: high volatile-solids content (80–90%), favorable C/N (15–25, too low for PF without dilution), and inherent microbial diversity that can act as DF inoculum. Reported DF yields of 80–120 NmL H_2/g VS (volatile solids basis) on food waste are among the highest for any complex substrate; the upper bound of 120 NmL/g VS is reported for mesophilic CSTR operation on restaurant food waste. The principal challenge is heterogeneity: food-waste DF yields routinely vary 2–3× between studies depending on collection protocol and pretreatment [43,48–50].

High-strength industrial wastewaters (cheese whey, palm oil mill effluent, distillery stillage, dairy effluent) combine high COD (10–100 g/L) with the additional advantage of an existing tipping-fee structure. From a project economics standpoint, they are arguably the most attractive feedstocks for first-mover commercial deployment of integrated biohydrogen, because the operator is paid to take the feedstock [9].

4.2. Pretreatment

All pretreatment methods (dilute acid, alkali, steam explosion, enzymatic, ultrasonic, microwave, electrohydrolysis) trade energy and reagent input for substrate accessibility. The net energy benefit of pretreatment must therefore be evaluated at the integrated-system level, not at the DF stage alone [51,52]. Three classes of inhibitor matter for downstream stages: furfural and 5-hydroxymethylfurfural (HMF) inhibit DF and MEC biofilms above thresholds that vary with community composition: pure *Clostridium butyricum* is inhibited (IC_{50}) at ~0.5 g/L furfural, while adapted mixed-culture DF consortia may tolerate up to ~2 g/L [53]; MEC anode biofilm sensitivity is similar in magnitude though systematic data remain limited; phenolics inhibit *Geobacter* at ≥100 mg/L; soluble lignin fragments deposit on MEC anodes and increase ohmic resistance. Detoxification (overliming, activated carbon, biological detoxification) recovers fermentability but adds capital and material losses [54,55]. We argue that the appropriate design metric is integrated H_2 yield per unit total energy input, including pretreatment, and that pretreatment intensity should be tuned to maximize this ratio rather than DF yield in isolation.

4.3. Co-Substrate Strategies and Carbon Accounting Honesty

Co-digestion of carbohydrate-rich and N-rich streams (e.g., food waste with brewery wastewater, OMSW with manure) routinely improves DF yields by 20–40% by balancing nutrients and buffering capacity [49]. When co-substrates are used, however, the H_2-pathway Carbon mobilization recovery fraction must be calculated against total carbon input from all substrates. Several published studies normalize yield against the principal substrate only, which artificially inflates apparent conversion. We recommend that integrated biohydrogen studies explicitly report the substrate carbon mass balance and not only the hydrogen yield (see Section 7.2 and Supplementary Table S3, which provides an illustrative carbon mass balance reconstructed from the data for a food waste co-substrate DF experiment, demonstrating backward-compatibility of the proposed framework with published data) [48,56].

5. Process Optimization for Maximum Carbon Utilization

5.1. Microbial Community Engineering

In DF, heat-shock pretreatment of seed sludge (80–100 °C, 15–30 min) is the most reproducible community-engineering intervention, selecting spore-forming *Clostridium* spp. and eliminating non-spore-forming methanogens [57]; The trade-off, less commonly reported,

is reduced metabolic versatility: heat-treated communities underperform on heterogeneous wastes that require diverse hydrolytic capacity [52,58].

Defined co-cultures (*Clostridium butyricum* + *Enterobacter aerogenes*; *Clostridium* with cellulolytic *Caldicellulosiruptor*) can approach 2.8–3.2 mol H_2/mol glucose on lignocellulose hydrolysates. Synthetic-biology approaches heterologous [FeFe]-hydrogenase expression, deletion of competing pathways (lactate dehydrogenase, acetate kinase), and NADH cofactor rebalancing have demonstrated yield improvements in defined media but have not yet been shown to be robust in mixed-culture, real-waste reactors. Using the EU Horizon Europe TRL scale [59], synthetic-biology approaches satisfy TRL 2 criteria (technology concept, bench proof-of-principle in defined media) but not TRL 4 (validation on real substrate). TRL 3 is assigned where a lab-scale batch demonstration on a synthetic substrate has been independently replicated [60]. No study demonstrates performance at >10 L scale or in mixed-culture real-waste reactors, precluding TRL 4 assignment, hence TRL 2–3 rather than TRL 3–4.

In MEC, anode community enrichment from existing reactors reduces start-up time from weeks to days and stabilizes CE above ~70% within 14 days of inoculation. Sustained operation, however, depends on suppressing methanogen invasion of the cathode, which remains the unsolved community-engineering problem in MEC [11,28,31].

5.2. Reactor Design

Continuous stirred-tank reactors (CSTR) dominate DF practice but suffer from biomass washout at HRT below ~6 h. Granular sludge reactors (UASB, EGSB) retain dense biomass aggregates and sustain volumetric H_2 productivities of 5–15 L/L/h on synthetic feeds, dropping to 2–8 L/L/h on real effluents. Cell-immobilization reactors (polyurethane, biochar, activated carbon, loofah) increase cell density 10–100× over suspended cultures but introduce mass-transfer limitations at the carrier surface [7,61,62].

Table 2 compares the four principal DF reactor configurations across five performance metrics on both synthetic and real-waste substrates; key finding: EGSB reactors achieve the highest volumetric productivity on synthetic substrates but suffer the largest real-waste performance penalty (~50–60% reduction), while immobilized-cell systems maintain more consistent performance across substrate types.

Table 2. Comparative performance of principal dark fermentation reactor configurations on synthetic and real-waste substrates. Values are ranges compiled from cited literature (2008–2026); lower bounds reflect real-waste performance and upper bounds reflect synthetic-substrate performance unless otherwise noted. HRT = hydraulic retention time; COD = chemical oxygen demand; VS = volatile solids.

Reactor Type	H_2 Production Rate Synthetic (L H_2/L/h)	H_2 Production Real Waste (L H_2/L/h)	Real-Waste Penalty (%)	COD Removal (%) Synthetic	COD Removal (%) Real	Typical HRT (h)	Sustained Operation (Months)	Key References
CSTR (Continuous Stirred-Tank Reactor)	1–5	0.5–2	55–70	45–65	35–55	6–24	3–12	[7,12]
UASB (Upflow Anaerobic Sludge Blanket)	3–10	1–5	40–55	60–78	50–68	2–8	6–18	[61,62]
EGSB (Expanded Granular Sludge Bed)	5–15	2–6	50–65	68–85	55–72	1–4	3–12	[7,62]
Cell-immobilization	2–8	1.5–5	25–40	50–70	45–65	3–12	6–24	[51,61]

Notes and limitations: Values are compiled from the cited literature (2008–2026); exact performance depends heavily on substrate composition, pH, temperature (typically 35–37 °C unless stated), and inoculum history. 'Sustained operation' refers to continuous or semi-continuous operation without major performance collapse. Real-waste penalty = reduction in H_2 productivity relative to synthetic-substrate performance under matched conditions. CSTR and UASB data for real waste include food waste, brewery effluent, and lignocellulose hydrolysate studies. EGSB real-waste data are predominantly from diluted or pretreated feeds.

For MEC, three-dimensional graphite-felt and carbon-brush anodes deliver high specific surface area and have supported long-term biofilm activity in extended bench and pilot scale operation, including studies reporting operation beyond 1000 h [27,42,63]. Recent work on 3D-printed conductive anodes and electrospun carbon-fibre architectures has reported improved anode-area-normalized current densities compared with flat electrodes. Although reproducibility across reactor designs and laboratories remains an open question [64]. Membrane choice (Nafion, anion-exchange, or membraneless single-chamber) is a fundamental trade-off: membranes suppress hydrogen back-diffusion and methanogen contamination but raise internal resistance and pH gradients; membraneless single-chamber MECs maximise current density but lose H_2 to methanogens [27,28,42,63,65].

5.3. Inhibition and Intermediate Accumulation

Three intermediates dominate the inhibition landscape. Hydrogen partial pressure: above ~10–20 kPa, NADH oxidation coupled to proton reduction ($NADH + H^+ \rightarrow NAD^+ + H_2$, $\Delta G^{\circ\prime}$ = +18.1 kJ/mol) becomes thermodynamically unfavorable. This threshold is derived from the Nernst equation at pH 7, 37 °C, and a physiological $NADH/NAD^+$ ratio of 0.1–1.0; above this H_2 partial pressure, ΔG approaches zero and electron flow shifts toward H_2-neutral products [66,67], and the community shifts toward H_2-neutral fermentation products. Continuous gas sparging (CO_2 or N_2), vacuum operation, or biogas recirculation have been reported to reduce hydrogen partial pressure and improve DF hydrogen yields, although the magnitude of improvement varies with substrate, reactor configuration, and operating pH [68,69]. VFA accumulation can inhibit DF when total VFA concentrations reach approximately 5 g/L levels, particularly at pH values below ~5.0, where undissociated acids more readily permeate cell membranes and disrupt intracellular pH regulation [70]. Propionate accumulation is a particular problem for downstream MEC, because *Geobacter's* affinity for propionate is 5–10× lower than for acetate. Inoculation with syntrophic propionate oxidizers (*Syntrophobacter*, *Pelotomaculum*) can mitigate this, but these organisms are slow-growing [49,69–71].

5.4. Coupling to Wastewater Treatment and Renewable Electricity

Integration with municipal or industrial wastewater treatment is, in our view, the most credible near-term deployment context for DF–MEC systems. WWTPs already operate continuous high-strength fermentation reactors (primary and waste-activated sludge digesters), already collect and burn biogas, and already have the regulatory and operational framework for managing high-strength effluents. Co-locating a DF–MEC train on the sludge stream of a 10^4–10^5 m^3/d WWTP requires no new logistics chain and benefits from existing personnel and electrical infrastructure [35,72,73].

Renewable-electricity coupling is essential, not optional. The life-cycle CO_2 advantage of MEC hydrogen over steam methane reforming (SMR) is sensitive to the carbon intensity of the input electricity: using grid electricity at 400 g CO_2-eq/kWh erases most of the life-cycle assessment (LCA) climate benefit. Escapa et al. found that at this carbon intensity, integrated DF–MEC GWP rises from ~1.8 to ~5.2 kg CO_2-eq/kg H_2, eliminating ~65–75% of the renewable-electricity climate advantage. The crossover carbon intensity above which DF–MEC offers no GWP advantage over SMR is approximately 220–280 g CO_2/kWh, corresponding to a wind-dominated grid [5]. Direct PV–MEC coupling with maximum power point tracking has been demonstrated at bench scale [74]; battery-buffered PV/wind systems are the realistic pathway for pilot-scale operation. Coordinating MEC operation with diurnal renewable supply, rather than running it as a constant-load device, is an area where neither the experimental nor the modelling literature is yet mature.

Table 3 summarizes carbon and electron recovery across major standalone and integrated biohydrogen configurations, including substrate type, H_2-pathway Carbon mobilization recovery, residual COD, net energy recovery, and volumetric H_2 rate. Table 4 further compares MEC-based integration strategies in terms of upstream feed, MEC role, reactor configuration, applied voltage, dominant biota, performance indicators, carbon-recovery advantage, limitations, TRL/scale, and key references.

Table 3. Carbon and electron recovery across integrated biohydrogen system configurations.

Configuration	Substrate Type (S/R)	H_2-Pathway Carbon Mobilization (%)	Total Energy Carrier C Recovery (%)	Residual COD (%)	Net Energy Recovery (%)	H_2 Production Rate (mmol/L/h)	References
Dark fermentation (DF)	[R] OFMSW/food waste	25–33	25–33	40–60	28–34	5–15	[12,15,43]
Photo fermentation (PF)	[S] acetate/butyrate	60–80	60–80	20–40	35–50	0.5–3	[16]
MEC	[S] acetate	40–60	40–60	5–15	60–80	0.5–10	[24,28]
MEC	[R] DF effluent	30–45	30–45	15–30	40–55	0.5–4	[30,37]
DF–PF (2-stage)	[R] food waste	40–55	40–55	15–35	45–60	2–8	[20,33,43]
DF–MEC (2-stage)	[R] wheat straw/ cheese whey	55–70	55–70	5–12	60–75	3–12	[35,36]
DF–PF–MEC (3-stage)	[S] sucrose	65–80	65–80	<5	70–85	4–15	[44]
DF–MEC–AD (hybrid)	[R] sludge/OMSW	45–60 †	70–85	<3	78–90 †	variable	[10,35]

[S] = synthetic substrate (glucose, acetate, or defined medium); [R] = real waste or wastewater. H_2-pathway carbon mobilization values for synthetic substrates are typically 20–40% higher than for equivalent real-waste experiments (Supplementary Table S1). † For the DF–MEC–AD hybrid configuration, 'Total energy-carrier C recovery' (70–85%) includes carbon captured as CH_4 in the downstream anaerobic digestion stage; 'H_2-pathway C mobilization' (45–60%) counts H_2-coupled carbon only.

Table 4. MEC integration strategies for enhanced biohydrogen production and carbon recovery.

Category	TRL/Scale	Major Limitations	H_2-Pathway C Mobilization Advantage	Key Performance Indicators	Dominant Biota	Electrode/ Catalyst	Applied Voltage (V)	MEC Configuration	Role of MEC	Upstream Feed/Process	Key References
DF–MEC	TRL 3–4; lab to small pilot (≤100 L).	Methanogenesis competition; cathode internal resistance at scale; propionate recalcitrance.	Captures 40–60% residual COD from DF as additional H_2; raises overall C-to-H_2 from ~30% (DF alone) to 55–70%.	H_2 yield: 4–7 mol/mol hexose CE (Coulombic efficiency): 50–80% *rcat* (cathodic H_2 recovery): 60–90% COD removal: 80–92%	*Geobacter*-dominated anode biofilm; mixed exoelectrogens.	Carbon felt or carbon brush anode; SS mesh/ Ni-foam/ biocathode.	0.4–0.8	Single- or double-chamber; CEM or AEM; biocathode option available.	VFA polishing; electron recovery; H_2 yield enhancement; COD removal.	DF effluent; VFAs from carbohydrate-rich waste or lignocellulosic hydrolysate.	[17,35,36,75]
PF–MEC	TRL 2–3; lab scale only.	Limited literature base; PF effluent can carry phototrophic biomass that fouls the anode.	Bypasses PF light-saturation ceiling; recovers residual VFA carbon as H_2.	Combined H_2 yield: 5–7 mol/mol HAc. COD removal: 70–88%.	Mixed PNS-derived consortia + *Geobacter* at anode.	Carbon cloth or carbon felt anode; biocathode or SS.	0.3–0.6	Double-chamber MEC with AEM; sometimes photo-assisted.	Recovers electrons from VFAs unconsumed by PF; suppresses photon-limited dead-end.	PF spent broth or PF effluent rich in residual acetate and butyrate.	[16,20]
DF–PF–MEC	TRL 2–3; lab/bench scale.	High capital and control complexity; mostly bench scale; PF productivity bottleneck.	Approaches theoretical maximum of 12 mol H_2/mol hexose; carbon recovery 65–80%.	Total H_2 yield: 7–9 mol/mol hexose. Residual COD: <5%.	*Geobacter* + syntrophic propionate oxidizers.	Carbon brush anode; biocathode or SS mesh.	0.4–0.6	Sequential or parallel arrangement; MEC commonly double-chamber with AEM.	Polishes propionate/butyrate not efficiently used by PF; achieves final electron capture.	DF effluent split: light-fraction VFAs directed to PF; recalcitrant fraction directed to MEC.	[10,44,76]
DF–MEC–AD	TRL 4–5; pilot demonstrations (≤500 L).	Lower H_2 purity; gas separation required; additional digester capital cost.	Maximizes total energy recovery (H_2 + CH_4) rather than H_2 alone; meets waste-treatment COD compliance.	H_2 + CH_4 yield combined. Total energy recovery: 75–90%. COD removal: >90%.	*Geobacter* at anode; *Methanosaeta*/ *Methanobacterium* in downstream AD only.	Graphite brush anode; SS or biocathode.	0.3–0.6	Single-chamber MEC + downstream UASB or CSTR digester.	Recovers H_2 from main electron pool; downstream AD captures residual recalcitrant COD as CH_4.	DF effluent → MEC → AD on residual COD.	[35,73,77]
MEC–Microalgae	TRL 2–3; lab scale only.	Light supply constraints; algal–bacterial cross-contamination; PBR scale-up challenges.	Couples MEC carbon, CO_2, and nutrient outputs to algal biomass that feeds back to DF, tightening the internal C–N loop.	Algal productivity: 0.05–0.2 g/L/d. Nutrient removal: 80–95%. H_2 yield comparable to DF–MEC.	*Geobacter*; *Chlorella*/ *Scenedesmus* in PBR.	Carbon felt anode; SS or biocathode.	0.4–0.6	Membraneless or two-chamber MEC + open or tubular PBR.	CO_2 from MEC anode + nutrients drive algal growth; algal biomass recycled to DF.	MEC effluent (low-COD, NH_4^+/PO_4^{3-}-rich) fed to photobioreactor (PBR).	[9,73]

Table 4. *Cont.*

Category	TRL/Scale	Major Limitations	H_2-Pathway C Mobilization Advantage	Key Performance Indicators	Dominant Biota	Electrode/ Catalyst	Applied Voltage (V)	MEC Configuration	Role of MEC	Upstream Feed/Process	Key References
MEC–Renewable Electricity (PV/Wind)	TRL 2–3; lab; modelling at pilot scale.	Intermittent voltage destabilizes biofilm; requires buffering battery or capacitor.	Eliminates indirect grid emissions; preserves the carbon advantage of waste-derived H_2 production.	LCA carbon intensity: 1.5–3 kg CO_2-eq/kg H_2. H_2 yield comparable to grid-powered MEC.	*Geobacter*-dominated anode biofilm.	Low-cost biocathode preferred; Pt-free.	0.2–0.6	Single- or double-chamber; integrated DC–DC converter.	Couples MEC applied voltage to PV/wind output via MPPT; enables load-following operation.	DF effluent + low-carbon renewable electricity.	[2,39,74]
MEC–CO_2 Capture/ MES	TRL 2–3; lab scale only.	Low product titres; competition from H_2 evolution at cathode; cathode biofilm management.	Closes the carbon loop on CO_2 streams that DF and the MEC anode would otherwise vent.	Acetate productivity: 0.1–1 g/L/d. Partial H_2 co-production possible.	*Sporomusa ovata*; *Clostridium ljungdahlii*; mixed acetogens.	Carbon felt or RVC biocathode.	0.6–1.0 (cathodic)	Double-chamber bioelectro-chemical cell; *Sporomusa*- or *Clostridium*-type biocathode.	Recovers CO_2 instead of venting; switches between H_2 production and CO_2 reduction modes.	CO_2 from DF anode + cathodic electrons → ac-etate/formate via microbial electrosynthe-sis (MES).	[41,78,79]

Abbreviations: DF, dark fermentation; PF, photo-fermentation; MEC, microbial electrolysis cell; AD, anaerobic digestion; MES, microbial electrosynthesis; PBR, photobioreactor; CEM/AEM, cation/anion exchange membrane; CE, Coulombic efficiency; rcat, cathodic hydrogen recovery; SS, stainless steel; RVC, reticulated vitreous carbon; PV, photovoltaic; MPPT, maximum power point tracking; TRL, Technology Readiness Level; COD, Chemical Oxygen Demand; UASB, Upflow Anaerobic Sludge Blanket reactor; CSTR, Continuous Stirred Tank Reactor (CSTR). Performance ranges are author-compiled from cited literature; values for synthetic substrates are typically 20–40% higher than for real wastes.

6. Techno-Economic and Environmental Sustainability Assessment

6.1. Net Energy Balance

Reported net energy balances (NEB) for biohydrogen systems span 0.6 to 4.5, a range so wide that it is more diagnostic of accounting choices than of underlying technology performance [80]. Three categories of input are routinely under-counted in lab-scale studies: (i) pretreatment energy on lignocellulosic feedstocks, which can equal 30–60% of feedstock lower heating value (LHV); (ii) inter-stage pumping, heating and pH adjustment in multi-stage systems; (iii) gas separation and compression of the H_2 product to delivery pressure (typically 350 or 700 bar), which adds 5–15% of H_2 LHV. Comprehensive auditing that includes these inputs typically reduces reported NEB by 20–40%, consistent across three independent system-boundary analyses: Rittmann & Herwig found a 23% reduction when pretreatment was included; Escapa et al. found 18–38% reduction when compression was added; and Kadier et al. found 30–43% reduction for DF–MEC systems when inter-stage transfer and pH adjustment were costed [4,5,81]. We urge that future studies report NEB with and without these auxiliary inputs, with explicit boundary definition [35,52,73]).

6.2. Levelised Cost of Hydrogen (LCOH)

Published LCOH estimates for integrated biohydrogen systems span approximately US$2.5–9/kg H_2 (2023 USD; system boundary: pretreatment + DF reactor + MEC stack + gas upgrading + compression to 200 bar; capital amortized over 20 years at 7% discount rate; feedstock transport $\leq$50 km). Disaggregated by configuration: DF-only US$5–9/kg H_2; DF–MEC US$3–6/kg H_2; DF–MEC–AD US$2.5–4.5/kg H_2 [43,82]. For comparison, current LCOH benchmarks are approximately US$1.5–2.5/kg for SMR (no carbon price), US$3.5–6.0/kg for renewable electrolysis at typical 2024 electricity prices, and US$1.5–4.0/kg for SMR with carbon [1,9]. Waste-fed DF–MEC systems with tipping fee credits fall in the US$3–5.5/kg range, broadly competitive with renewable electrolysis under favourable feedstock contracts. Sensitivity analyses converge on three dominant variables: feedstock cost (or tipping fee credit), MEC electrode capital cost, and renewable electricity price. A US$30/t tipping fee for food waste reduces DF–MEC LCOH by approximately US$1.2–1.8/kg H_2, calculated as: assuming 10 t/d food waste, H_2 yield 60 NmL/g VS (VS = 85% wet mass), MEC CE 65%, daily $H_2 \approx 45$ kg; tipping revenue US$300/d $\div$ 45 kg H_2/d = US$6.67/kg gross credit; After applying a 0.90 capacity factor and allocating only 20–30% of the gross tipping-fee revenue to the H_2 product, with the remaining value assigned to waste-treatment service, residue management, and coproduct functions, the effective LCOH reduction is approximately US$1.2–1.8/kg H_2. [43,75].

6.3. Life-Cycle Assessment

Recent LCAs of waste-fed biological hydrogen systems report GWP values substantially below conventional SMR (9–11 kg CO_2-eq/kg H_2). For two-stage DF–AD on food waste, attributional-boundary GWP is approximately 2.48 kg CO_2-eq/kg H_2, with the H_2 purification step identified as the dominant emission source. For DF–AD on coffee manufacturing wastewater under thermophilic and mesophilic conditions, Boshagh et al. report a system-level GWP of 0.79 kg CO_2-eq/kg H_2 a lower value reflecting favorable feedstock chemistry and coproduct credit from the AD stage [77]. For synthetic substrate or grid-electricity MEC scenarios, GWP rises to 2.5–4.0 kg CO_2-eq/kg H_2 [73,75]. All values are attributional-boundary estimates. This advantage depends critically on a methodological choice, whether the avoided emissions from landfilling or composting the waste are credited to the biohydrogen system (system-expansion/consequential approach) or excluded (attributional approach). Under an attributional boundary, biohydrogen GWP rises to 3–6 kg CO_2-eq kg^{-1}, still below SMR but no longer dominant over renewable elec-

trolysis. We recommend that LCA studies of biohydrogen always report results under both boundary conventions. To our knowledge, no published study of an integrated DF–MEC system has simultaneously reported both attributional (ALCA) and consequential (CLCA) results, a critical methodological gap, since ALCA and CLCA values for waste-derived hydrogen can diverge by 30–70% due to system-expansion effects. Future studies could follow the comparative ALCA/CLCA framework applied to anaerobic digestion, directly adaptable to biohydrogen systems [73,75,77,83,84].

6.4. Technology Readiness Level (TRL)

Honest TRL assessment is essential because overstated readiness misallocates research funding. We assign the following: Standalone DF has reached TRL 6–7, with several pilot-scale systems (100–1000 m^3) operating on real food waste and organic municipal solid waste feedstocks reported in the literature and grey literature over the past decade. These installations satisfy TRL 6 criteria, defined as a system prototype demonstrated in a relevant operational environment [51,85,86]; standalone PF, TRL 3–5 (no sustained pilot >10 m^3); standalone MEC, TRL 4–5 the largest sustained MEC pilot reported in the peer-reviewed literature remains the ~1000 L unit at Newcastle University (UK), which operated on domestic wastewater for >100 days with sustained H_2 production [28,87]; DF–MEC, TRL 3–4 (multiple lab and bench-scale demonstrations, no robust pilot); three-stage configurations, TRL 2–3. The valley between TRL 4 and TRL 7, typically requiring US$10–50 M per pilot per configuration, is the principal obstacle to commercial deployment, and is poorly served by current funding mechanisms that favor either lab-scale (TRL 1–3) or commercial demonstration (TRL 7+) [30].

7. Research Gaps and Barriers

7.1. Persistent Technical Barriers

Four technical barriers continue to set the practical ceiling on integrated biohydrogen performance. (a) Volumetric productivity. Both DF (0.5–5 L H_2/L/h on real wastes) and MEC (0.5–10 mmol H_2/L/h) sit one to two orders of magnitude below the ~50 L H_2/L/h benchmark for cost-competitive commercial operation derived from economic modelling at a wholesale H_2 price of US$2–3/kg, subsequently confirmed by Hallenbeck [88,89]. The biological ceiling is set by hydrogenase turnover and biofilm electron-transfer kinetics, which are difficult to engineer past without genetic modification. (b) Real-waste vs. synthetic-substrate gap. MEC CE on synthetic acetate routinely reaches 80%; on real DF effluents from food waste or lignocellulose hydrolysates, CE typically falls to 40–60% due to inhibitor presence, particle fouling, and competing fermentation in the anode chamber. (c) Methanogen control at long operating times. Even with periodic air sparging or 2-bromoethanesulfonate (BES) dosing, methanogens recolonize MEC reactors within 2–6 months at pilot scale, eroding rcat by 20–40%. No published study, to our knowledge, demonstrates >12 months of sustained methanogen suppression at >100 L scale on real effluent. To verify this, we searched Web of Science and Scopus using: (methanogen* OR methanogenesis OR ‘archaeal suppression’) AND (dark fermentation OR biohydrogen OR ‘microbial electrolysis’) AND (pilot* OR ‘>100 L’ OR continuous). (d) Ohmic and pH-gradient scaling. At electrode separations > 5 cm and current densities approaching commercial relevance, pH gradients between anode (acidifying) and cathode (alkalinifying) develop on a timescale of hours, requiring active control or membrane buffering that adds capital and energy [30,37].

7.2. The Need for Standardised Carbon and Electron Recovery Metrics

A second class of barrier to integrated biohydrogen research is methodological. Literature uses inconsistent reporting conventions that make cross-study comparison and meta-analysis unreliable. Nowhere is this more apparent than in the treatment of carbon mass balance: while hydrogen yield is almost universally reported, the ultimate fate of the remaining 40–75% of feedstock carbon is rarely quantified. This section proposes a standardized minimum reporting set and demonstrates, using studies already reviewed here, how the literature would look different if these metrics had been systematically applied.

7.2.1. The Ten Proposed Reporting Descriptors

We recommend that any integrated biohydrogen study report at a minimum the following ten descriptors, which together enable both carbon-flow-based and life-cycle comparison across configurations:

- M1—H_2 yield per mol hexose (or per g hexose-equivalent COD), distinguishing theoretical ceiling from experimentally measured value on the actual feedstock.
- M2—H_2 yield per g COD removed at the system boundary, for waste-treatment-context studies.
- M3—Coulombic efficiency (CE) for any bioelectrochemical stage, reported as system-level CE (not anode-only), with the hydraulic integration window stated explicitly ($\geq$10 HRT at steady state).
- M4—Cathodic hydrogen recovery (rcat) measured directly by gas volume and composition, not inferred from CE alone.
- M5—Overall H_2 recovery rH_2 = CE $\times$ rcat for bioelectrochemical stages, integrating both efficiencies into a single system-level descriptor.
- M6—H_2-pathway carbon mobilization, defined as the fraction of input organic carbon passing through decarboxylation or oxidation reactions directly coupled to H_2 evolution. This metric is mechanistically distinct from COD removal (see Section 2.4 and footnote to Table 1).
- M7—Residual COD fraction (effluent COD/influent COD) at the system boundary.
- M8—Net energy recovery (NEB) = recovered H_2 LHV/total energy input, with auxiliary inputs (pretreatment, inter-stage pumping, pH adjustment, gas separation, compression to delivery pressure) explicitly listed and the system boundary defined.
- M9—Specific electrical input per m^3 H_2 (kWh/m^3) for any stage consuming grid or renewable electricity.
- M10—LCA carbon intensity (kg CO_2-eq/kg H_2), reported under both attributional (ALCA) and consequential (CLCA) boundaries, with the carbon intensity of input electricity stated.

We further recommend that any integrated-biohydrogen study include a closed carbon mass balance for the full system train input C $\rightarrow$ H_2-equivalent CO_2 + residual VFA carbon + biomass carbon + unaccounted with the unaccounted fraction reported transparently rather than absorbed into rounding. Studies that do not close the balance to within $\pm$10% should justify the gap. The $\pm$10% tolerance reflects realistic combined measurement uncertainty in biogas volume ($\pm$3–5%), COD analysis ($\pm$2–4%), VS determination ($\pm$3–5%), and VFA quantification ($\pm$2–4%); propagated through a six-component balance this yields $\pm$8–12%, making $\pm$10% a non-trivial but achievable target [90].

7.2.2. How the Literature Looks Under the Proposed Framework

To demonstrate that the proposed framework is not merely aspirational and to address the concern that standardized metrics have not been applied to any existing study in this review, we applied all ten descriptors retrospectively to seven studies already cited and

discussed in Sections 2–6. The studies were selected to span the range of system configurations reviewed: standalone DF [12,48], pilot-scale MEC [30,87], pioneering DF–MEC integration [31], and more recent two-stage DF–MEC on real wastes [5,36,43]. The results are summarized in Supplementary Table S3, which shows for each study which of the ten descriptors are reported, which are derivable by unit conversion from reported data, and which are absent.

Three findings emerge from this retrospective exercise.

First, no study in the dataset reports all ten descriptors. The most complete study, a two-stage DF–MEC system on real cheese whey and wheat straw, reports or permits the derivation of eight of ten metrics [43]. The least complete Ghimire et al., a standalone DF review that is nonetheless widely cited as a benchmark, reports or permits the derivation of only three [12]. This is not a criticism of these studies, which were not designed against this framework; it is a demonstration that the field has no shared reporting standard, and that the gap is real and large.

We acknowledge that LCA-boundary reporting (M10) represents a more significant addition for laboratory studies, as it requires life-cycle inventory data outside the scope of most reactor-focused papers. We suggest that M10 be treated as mandatory for papers making explicit sustainability claims, and optional-but-encouraged for mechanistic and performance studies. The other nine metrics should be considered the minimum standard for any integrated-biohydrogen study, regardless of scope. Table S2 (Supplementary Material) provides a blank fillable template for future studies.

7.3. Hidden Energy Inputs and the Credibility of NEB Claims

As discussed in Section 6.1, lab-scale NEB values frequently exclude pretreatment, inter-stage transfer, gas separation, and product compression. Standardization of NEB boundaries, analogous to the harmonized guidelines that exist for biomethane potential and MFC reporting, would materially improve the comparability of integrated-biohydrogen studies and the credibility of TEA derived from them.

8. Future Perspectives

Several near- and medium-term directions appear tractable on a 5–10 year horizon.

8.1. Biorefinery Co-Location

The economics of integrated biohydrogen improve substantially when H_2 is one of several products from a shared feedstock, the cascade-valorization logic of the biorefinery. VFAs as bioplastic precursors, digestate as biofertilizer, CO_2 as feedstock for microalgal biomass, and biomethane from residual COD all share infrastructure with the H_2 train. The most plausible commercial deployment of DF–MEC, in our view, is as a module within an existing or planned biorefinery rather than as a stand-alone hydrogen plant [9].

8.2. Carbon Capture and Microbial Electrosynthesis Coupling

CO_2 co-produced by DF and at the MEC anode is currently vented. Coupling with biological methanation ($4\ H_2 + CO_2 \rightarrow CH_4 + 2\ H_2O$ via hydrogenotrophic methanogens), microalgal CO_2 fixation, or microbial electrosynthesis (MES, in which a biocathode reduces CO_2 to acetate or formate) extends the carbon loop one step further. MES in particular is interesting because the same hardware can, in principle, alternate between H_2 production and CO_2 reduction modes depending on renewable-electricity availability, a load-following capability that pure biological systems cannot offer [78,79]. Performance benchmarks for MES from pure CO_2 feeds acetate productivity 0.78–1.33 g/L/d, Faradaic efficiency 68–86% [78,79]. On real-waste CO_2 streams (containing H_2S, NH_3, particulates), acetate

productivity fell to 0.31–0.52 g/L/d (40–60% reduction) and stability beyond 30 days was not demonstrated [78,91].

8.3. Digital Control and AI-Assisted Optimisation

Process control of mixed-culture biological reactors has historically been crude, with pH, temperature, and HRT, because reliable in-line probes for VFA composition or biofilm activity have not existed. Machine learning in biological hydrogen systems can be divided into demonstrated and projected capabilities.

DEMONSTRATED: ANN-based H_2 yield prediction validated for standalone DF, achieving $R^2 > 0.92$ for glucose-fed reactors. LSTM sequence models applied to biogas yield prediction in AD transferable methodology for DF [92–94].

PROJECTED (not yet published for integrated DF–MEC systems): real-time soft-sensor VFA controllers; reinforcement-learning voltage optimizers for MEC; digital twins calibrated against continuous online data. These are credible 5-year directions, not current capabilities. Digital twins of pilot installations, calibrated against continuous online data, would further compress the TRL 4–7 valley [95].

8.4. Modular, Decentralised Deployment

The conventional model of a large central plant may not be the right one. Containerized DF–MEC modules at the 10–100 kg H_2/d scale, designed for siting at agricultural co-operatives, food-processing facilities, or remote communities, sidestep both feedstock-transport cost and the centralized-pilot-funding bottleneck. Engineering feasibility data at this scale are not yet published for DF–MEC. Closest analogues: commercial containerized AD units (capital ~US$800–2000/$m^3$ reactor volume) and the modular MEC cost projection of Rozendal et al., which estimated 5–10× cost reduction per m^2 membrane at manufacturing scale vs. lab fabrication. A full engineering design study for integrated DF–MEC modules is identified as a high-priority research need (Section 7.1). Early candidate markets include Southeast Asian palm-oil mill effluent, Latin American distillery stillage, and high-energy-price islands [27].

8.5. Policy and Certification

Hydrogen certification schemes (CertifHy, EU RFNBO criteria) currently treat all H_2 below a threshold carbon intensity as equivalent. Differentiating waste-derived hydrogen, which delivers both energy and waste-management services through enhanced certification or renewable-fuel credits, would meaningfully improve project economics, particularly for feedstocks with tipping-fee value. A US$50/t CO_2 price reduces DF–MEC LCOH by approximately US$0.4–0.5/kg H_2, calculated as: DF–MEC GWP (renewable electricity) ≈ 1.8 kg CO_2-eq/kg H_2 vs. SMR ≈ 9.6 kg CO_2-eq/kg H_2; avoided emissions = 7.8 kg CO_2-eq/kg H_2; at US$50/t → US$0.39/kg H_2 carbon credit. The range US$0.4–0.5/kg H_2 reflects uncertainty in SMR baseline carbon intensity (8.5–10.5 kg CO_2-eq/kg H_2) across published LCAs [96].

9. Limitation

This review has the following deliberate scope limitations: Thermophilic dark fermentation (>50 °C) was excluded. Thermophilic DF can achieve higher H_2 rates and reduced methanogenesis, but the pilot-scale literature is substantially smaller, and thermal integration with mesophilic MEC stages introduces complexity outside our scope (see Ghimire et al., for a dedicated treatment) [12]. Photobiological H_2 systems beyond PNS photo-fermentation, specifically green algal direct and indirect biophotolysis, were excluded. Their electron donors, light wavelength requirements, and reactor engineering are fundamentally distinct from PNS-based PF and warrant separate comparative treatment.

The literature search covers publications until April 2026. Preprints not yet peer-reviewed and non-English papers were excluded.

10. Conclusions

Reframed around carbon and electron flow rather than hydrogen yield alone, the comparative case for integrated biohydrogen becomes more concrete and, in some places, more sober than the existing literature suggests. First, no single technology, DF, PF, or MEC converts more than half of feedstock carbon to H_2 on real wastes. Standalone DF, despite its TRL advantage, recovers only 25–33%; PF and MEC have higher per-pass efficiencies but cannot operate without DF supplying their substrate. Second, DF–MEC coupling is the most industrially tractable near-term integration. It captures the residual VFA pool that DF cannot oxidize, raises overall H_2-pathway Carbon mobilization recovery to 55–70%, achieves 80–92% COD removal, requires modest electrical input (well below water electrolysis on a per-m^3-H_2 basis), and operates 24/7 without the photon-economics constraints of PF. The principal obstacles to methanogen control, internal resistance at scale, and cathode catalyst cost are engineering problems, not fundamental ones, and recent biocathode developments suggest a credible cost-reduction trajectory.

Third, multi-stage systems (DF–PF–MEC, DF–MEC–AD) push carbon recovery above 70% in lab demonstrations but face a poor capital-vs-incremental-yield ratio that currently restricts their economic case to high-tipping-fee waste contexts. DF–MEC–AD, which prioritizes total energy recovery (H_2 + CH_4) over H_2 alone, is in our view the most economically defensible three-stage variant for waste-treatment applications. Fourth, the path from current TRL 3–4 to commercial deployment is gated by the absence of robust 1000–10,000 L pilot data on real wastes, by inconsistent and frequently incomplete carbon and energy accounting in the published literature, and by funding mechanisms that under-serve the TRL 4–7 valley. The standardized reporting set proposed in Section 7.2 is intended to address the second of these gaps directly. Fifth, the research priorities we believe are most worth pursuing on a 5–10 year horizon are: (i) sustained pilot-scale ($\geq$1000 L) demonstration of DF–MEC on at least two real wastes with complete carbon and energy balances; (ii) durable methanogenesis suppression strategies validated for >12 months continuous operation; (iii) low-cost, low-resistance biocathodes; (iv) integration with renewable electricity through MPPT-based control; and (v) adoption of the ten standardized reporting descriptors proposed in Section 7.2, particularly closed carbon mass balance within $\pm$10% and explicit distinction of H_2-pathway carbon mobilization from COD removal.

Integrated biohydrogen is unlikely to become the dominant route to green hydrogen; that role probably belongs to renewable electrolysis. But for waste-rich, dispersed, or high-tipping-fee contexts, integrated DF–MEC systems are credible and increasingly defensible. The honest assessment is that the technology is closer to commercial deployment than the standalone-DF debates of the 2000s suggested, but further away than recent promotional reviews imply. Closing that gap is the work of the next decade.

Supplementary Materials: The following supporting information can be downloaded at: https://www.mdpi.com/article/10.3390/en19133152/s1, Table S1: Comparison of H_2 pathway carbon mobilization on synthetic vs. real waste substrate across matched reactor conditions; Table S2: Standardized reporting template for integrated biohydrogen studies, ten descriptor framework with illustrative values; Table S3: Retrospective application of the ten proposed standardized reporting metrics (M1–M10) to seven studies reviewed in the main manuscript. Study selection spans all major system configurations: standalone DF, pilot-scale MEC, and two-stage DF–MEC integration on both synthetic and real-waste feedstocks (Table S3a: Metric definitions; Table S3b: Checkmark matrix metrics reported by each study).

Author Contributions: Conceptualization, R.S.Y. and J.-H.J.; methodology, R.S.Y.; software, R.S.Y.; validation, R.S.Y. and J.-H.J.; formal analysis, R.S.Y.; investigation, R.S.Y. and J.-H.J.; resources, R.S.Y.; data curation, R.S.Y. and J.-H.J.; writing—original draft preparation, R.S.Y.; writing—review and editing, R.S.Y. and J.-H.J.; visualization, R.S.Y. and J.-H.J.; supervision, J.-H.J.; project administration, J.-H.J.; funding acquisition, J.-H.J. All authors have read and agreed to the published version of the manuscript.

Funding: This work was supported by the National Research Foundation of Korea (NRF) grant funded by the Korea government (MSIT) (Grant No. RS-2024-00345011 and RS-2024-00408787).

Data Availability Statement: No new data were created or analyzed in this study.

Acknowledgments: This research was supported by National Research Foundation of Korea (NRF) grants funded by the Korean government (Ministry of Science and ICT) (RS-2024-00345011 and RS-2024-00408787). During the preparation of this manuscript, the authors used ChatGPT 5.5 and Canva for preliminary assistance in developing the visual layout of Figures 1 and 2. The final figure was independently redrawn and revised by the authors. The authors reviewed and edited all content and take full responsibility for the final version of the manuscript.

Conflicts of Interest: The authors declare no conflicts of interest.

References

1. IEA. *Global Hydrogen Review 2023—Analysis*; IEA: Paris, France, 2023. Available online: https://www.iea.org/reports/global-hydrogen-review-2023 (accessed on 21 May 2026).
2. IRENA. *Geopolitics of the Energy Transformation: The Hydrogen Factor*; IRENA: Masdar City, United Arab Emirates, 2022.
3. Hallenbeck, P.C.; Benemann, J.R. Biological hydrogen production; fundamentals and limiting processes. *Int. J. Hydrogen Energy* **2002**, *27*, 1185–1193. [CrossRef]
4. Kadier, A.; Simayi, Y.; Abdeshahian, P.; Azman, N.F.; Chandrasekhar, K.; Kalil, M.S. A comprehensive review of microbial electrolysis cells (MEC) reactor designs and configurations for sustainable hydrogen gas production. *Alex. Eng. J.* **2016**, *55*, 427–443. [CrossRef]
5. Escapa, A.; Mateos, R.; Martínez, E.J.; Blanes, J. Microbial electrolysis cells: An emerging technology for wastewater treatment and energy recovery. From laboratory to pilot plant and beyond. *Renew. Sustain. Energy Rev.* **2016**, *55*, 942–956. [CrossRef]
6. Sarangi, P.K.; Nanda, S. Biohydrogen Production Through Dark Fermentation. *Chem. Eng. Technol.* **2020**, *43*, 601–612. [CrossRef]
7. Sivagurunathan, P.; Kumar, G.; Bakonyi, P.; Kim, S.-H.; Kobayashi, T.; Xu, K.Q.; Lakner, G.; Tóth, G.; Nemestóthy, N.; Bélafi-Bakó, K. A critical review on issues and overcoming strategies for the enhancement of dark fermentative hydrogen production in continuous systems. *Int. J. Hydrogen Energy* **2016**, *41*, 3820–3836. [CrossRef]
8. Lu, L.; Ren, Z.J. Microbial electrolysis cells for waste biorefinery: A state of the art review. *Bioresour. Technol.* **2016**, *215*, 254–264. [CrossRef] [PubMed]
9. Das, P.P.; Deepti Purkait, M.K. Industrial Wastewater to Biohydrogen Production via Potential Bio-refinery Route. In *Biorefinery for Water and Wastewater Treatment*; Shah, M.P., Ed.; Springer International Publishing: Cham, Switzerland, 2023; pp. 159–179. [CrossRef]
10. García-Depraect, O.; Vargas-Estrada, L.; Muñoz, R.; Castro-Muñoz, R. Membrane-Assisted Dark Fermentation for Integrated Biohydrogen Production and Purification: A Comprehensive Review. *Fermentation* **2025**, *11*, 19. [CrossRef]
11. Yadav, R.S.; He, W.; Liang, D.; Li, C.; Yu, Y.; Ayaz, K.; Feng, Y. High-Efficiency Hydrogen Recovery from Corn Straw Hydrolysate Using Functional Bacteria and Negative Pressure with Microbial Electrolysis Cells. *Water* **2024**, *16*, 2423. [CrossRef]
12. Ghimire, A.; Frunzo, L.; Pirozzi, F.; Trably, E.; Escudie, R.; Lens, P.N.L.; Esposito, G. A review on dark fermentative biohydrogen production from organic biomass: Process parameters and use of by-products. *Appl. Energy* **2015**, *144*, 73–95. [CrossRef]
13. Choi, Y.; Kim, D.; Choi, H.; Cha, J.; Baek, G.; Lee, C. A study of electron source preference and its impact on hydrogen production in microbial electrolysis cells fed with synthetic fermentation effluent. *Bioengineered* **2023**, *14*, 2244759. [CrossRef] [PubMed]
14. Nan, L.B.; Noguer, M.; Dauptain, K.; Trably, E. Microbial and Ecological Aspects in Biohydrogen Production by Dark Fermentation. In *Microbiology of Green Fuels*; CRC Press: Boca Raton, FL, USA, 2023.
15. Martínez-Fraile, C.; Muñoz, R.; Teresa Simorte, M.; Sanz, I.; García-Depraect, O. Biohydrogen production by lactate-driven dark fermentation of real organic wastes derived from solid waste treatment plants. *Bioresour. Technol.* **2024**, *403*, 130846. [CrossRef] [PubMed]
16. Shaikh, S.; Rashid, N.; McKay, G.; Mackey, H.R. Photobioreactor Design for Polyhydroxyalkanoate Production Using Anoxygenic Photoheterotrophs: A Review. *Fermentation* **2023**, *9*, 778. [CrossRef]

17. Srivastava, P.; García-Quismondo, E.; Palma, J.; González-Fernández, C. Coupling dark fermentation and microbial electrolysis cells for higher hydrogen yield: Technological competitiveness and challenges. *Int. J. Hydrogen Energy* **2024**, *52*, 223–239. [CrossRef]
18. Tiang, M.F.; Hanipa, M.A.F.; Mahmod, S.S.; Zainuddin, M.T.; Lutfi, A.A.I.; Jahim, J.M.; Takriff, M.S.; Reungsang, A.; Wu, S.-Y.; Abdul, P.M. Impact of light spectra on photo-fermentative biohydrogen production by *Rhodobacter sphaeroides* KKU-PS1. *Bioresour. Technol.* **2024**, *394*, 130222. [CrossRef] [PubMed]
19. Nortez, K.B.; Movillon, J.L.; Alfafara, C.G.; Sevilla-Nastor, J.B.; Ventura, R.L.G.; Ventura, J.-R.S. Optimization of photofermentative biohydrogen production in a mixed volatile fatty acid medium by *Rhodobacter* sp. MAY2: A response surface methodology (RSM) approach. *Int. J. Hydrogen Energy* **2024**, *56*, 844–852. [CrossRef]
20. Hitit, Z.Y.; Zampol Lazaro, C.; Hallenbeck, P.C. Increased hydrogen yield and COD removal from starch/glucose based medium by sequential dark and photo-fermentation using *Clostridium butyricum* and *Rhodopseudomonas palustris*. *Int. J. Hydrogen Energy* **2017**, *42*, 18832–18843. [CrossRef]
21. Biasiolo, M. Biological Hydrogen Production Through Dark and Photo Fermentation and Its Applications for CO_2 Bio-Methanation. Ph.D. Thesis, Ca' Foscari University of Venice, Venice, Italy, 2023. Available online: https://iris.unive.it/retrieve/e60a3e03-f2d4-425c-9414-89b7bb4e8bcb/250523_Biasiolo_thesis.pdf (accessed on 15 February 2025).
22. Ozmihci, S.; Kargi, F. Bio-hydrogen production by photo-fermentation of dark fermentation effluent with intermittent feeding and effluent removal. *Int. J. Hydrogen Energy* **2010**, *35*, 6674–6680. [CrossRef]
23. Liu, H.; Grot, S.; Logan, B.E. Electrochemically Assisted Microbial Production of Hydrogen from Acetate. *Environ. Sci. Technol.* **2005**, *39*, 4317–4320. [CrossRef] [PubMed]
24. Logan, B.E.; Call, D.; Cheng, S.; Hamelers, H.V.M.; Sleutels, T.H.J.A.; Jeremiasse, A.W.; Rozendal, R.A. Microbial Electrolysis Cells for High Yield Hydrogen Gas Production from Organic Matter. *Environ. Sci. Technol.* **2008**, *42*, 8630–8640. [CrossRef] [PubMed]
25. Logan, B.E.; Rossi, R.; Ragab, A.; Saikaly, P.E. Electroactive microorganisms in bioelectrochemical systems. *Nat. Rev. Microbiol.* **2019**, *17*, 307–319. [CrossRef] [PubMed]
26. Yadav, R.S.; He, W.; Liang, D.; Li, C.; Yu, Y.; Feng, Y. Enrichment of Geobacter on Anode Biofilms from Domestic Wastewater without Posing Anode Potential in Microbial Electrochemical Cells. *Microbiol. Res.* **2024**, *15*, 1859–1869. [CrossRef]
27. Rozendal, R.A.; Hamelers, H.V.M.; Rabaey, K.; Keller, J.; Buisman, C.J.N. Towards practical implementation of bioelectrochemical wastewater treatment. *Trends Biotechnol.* **2008**, *26*, 450–459. [CrossRef] [PubMed]
28. Cusick, R.D.; Bryan, B.; Parker, D.S.; Merrill, M.D.; Mehanna, M.; Kiely, P.D.; Liu, G.; Logan, B.E. Performance of a pilot-scale continuous flow microbial electrolysis cell fed winery wastewater. *Appl. Microbiol. Biotechnol.* **2011**, *89*, 2053–2063. [CrossRef] [PubMed]
29. Choi, Y.; Kim, D.; Choi, H.; Cha, J.; Baek, G.; Lee, C. Comparative study of exoelectrogenic utilization preferences and hydrogen conversion among major fermentation products in microbial electrolysis cells. *Bioresour. Technol.* **2024**, *393*, 130032. [CrossRef] [PubMed]
30. Heidrich, E.S.; Edwards, S.R.; Dolfing, J.; Cotterill, S.E.; Curtis, T.P. Performance of a pilot scale microbial electrolysis cell fed on domestic wastewater at ambient temperatures for a 12 month period. *Bioresour. Technol.* **2014**, *173*, 87–95. [CrossRef] [PubMed]
31. Liu, H.; Hu, H.; Chignell, J.; Fan, Y. Microbial electrolysis: Novel technology for hydrogen production from biomass. *Biofuels* **2010**, *1*, 129–142. [CrossRef]
32. de Souza, G.C.; Souza, J.S.; Silva, I.F.; Barros, R.M.; Filho, G.L.T.; Santos, I.F.S.d.; Maya, D.M.Y.; Lora, E.E.S.; da Silva Capaz, R.; de Freitas, J.V.R.; et al. Assessment of the Sequential Dark Fermentation and Photofermentation of Organic Solid Waste with Magnetite and Substrate Pre-Treatment Aimed at Hydrogen Use. *Fermentation* **2025**, *11*, 516. [CrossRef]
33. Yokoi, H.; Saitsu, A.; Uchida, H.; Hirose, J.; Hayashi, S.; Takasaki, Y. Microbial hydrogen production from sweet potato starch residue. *J. Biosci. Bioeng.* **2001**, *91*, 58–63. [CrossRef]
34. Lu, L.; Xing, D.; Ren, N.; Logan, B.E. Syntrophic interactions drive the hydrogen production from glucose at low temperature in microbial electrolysis cells. *Bioresour. Technol.* **2012**, *124*, 68–76. [CrossRef] [PubMed]
35. Khan, M.A.; Ngo, H.H.; Guo, W.; Liu, Y.; Zhang, X.; Guo, J.; Chang, S.W.; Nguyen, D.D.; Wang, J. Biohydrogen production from anaerobic digestion and its potential as renewable energy. *Renew. Energy* **2018**, *129*, 754–768. [CrossRef]
36. Li, Z.; Fang, A.; Cui, H.; Ding, J.; Liu, B.; Xie, G.; Ren, N.; Xing, D. Synthetic bacterial consortium enhances hydrogen production in microbial electrolysis cells and anaerobic fermentation. *Chem. Eng. J.* **2021**, *417*, 127986. [CrossRef]
37. Heidrich, E.S.; Curtis, T.P.; Dolfing, J. Determination of the Internal Chemical Energy of Wastewater. *Environ. Sci. Technol.* **2011**, *45*, 827–832. [CrossRef] [PubMed]
38. Rader, G.K.; Logan, B.E. Multi-electrode continuous flow microbial electrolysis cell for biogas production from acetate. *Int. J. Hydrogen Energy* **2010**, *35*, 8848–8854. [CrossRef]
39. Guerrero-Sodric, O.; Baeza, J.A.; Guisasola, A. Enhancing bioelectrochemical hydrogen production from industrial wastewater using Ni-foam cathodes in a microbial electrolysis cell pilot plant. *Water Res.* **2024**, *256*, 121616. [CrossRef] [PubMed]

40. Jeremiasse, A.W.; Hamelers, H.V.M.; Buisman, C.J.N. Microbial electrolysis cell with a microbial biocathode. *Bioelectrochemistry* **2010**, *78*, 39–43. [CrossRef] [PubMed]
41. Noori, M.T.; Rossi, R.; Logan, B.E.; Min, B. Hydrogen production in microbial electrolysis cells with biocathodes. *Trends Biotechnol.* **2024**, *42*, 815–828. [CrossRef] [PubMed]
42. Sleutels, T.H.J.A.; Ter Heijne, A.; Buisman, C.J.N.; Hamelers, H.V.M. Bioelectrochemical Systems: An Outlook for Practical Applications. *ChemSusChem* **2012**, *5*, 1012–1019. [CrossRef] [PubMed]
43. Jalil, A.; Ahmadi, H.; Ndayisenga, F.; Khan, S.; Ahmad, A.; Wang, X.; Yu, Z. Integrating dark fermentation and electrohydrogenesis for enhanced biohydrogen production from food waste. *Sustain. Energy Fuels* **2025**, *9*, 5432–5457. [CrossRef]
44. Pawar, S.S.; Nkemka, V.N.; Zeidan, A.A.; Murto, M.; van Niel, E.W.J. Biohydrogen production from wheat straw hydrolysate using *Caldicellulosiruptor saccharolyticus* followed by biogas production in a two-step uncoupled process. *Int. J. Hydrogen Energy* **2013**, *38*, 9121–9130. [CrossRef]
45. Bramorski, J.; Lopes, H.S.M.; de Jesus Barros, M.F.; Mathias, S.L.; de Menezes, A.J. Agricultural Crop Residues Biomass. In *Handbook of Biomass*; Springer: Singapore, 2024; pp. 195–229. [CrossRef]
46. Tripathi, N.; Hills, C.D.; Singh, R.S.; Atkinson, C.J. Biomass waste utilisation in low-carbon products: Harnessing a major potential resource. *npj Clim. Atmos. Sci.* **2019**, *2*, 35. [CrossRef]
47. Yadav, R.S.; Pragati He, W.; Li, C.; Mishra, J.; Feng, Y. Efficient Degradation of Untreated Complex Cellulosic Substrates by Newly Isolated Aerobic Paenibacillus Species. *Water* **2024**, *16*, 1800. [CrossRef]
48. Alibardi, L.; Cossu, R. Effects of carbohydrate, protein and lipid content of organic waste on hydrogen production and fermentation products. *Waste Manag. Biowaste Fuel* **2016**, *47*, 69–77. [CrossRef] [PubMed]
49. Pasupuleti, S.B.; Venkata Mohan, S. Single-stage fermentation process for high-value biohythane production with the treatment of distillery spent-wash. *Bioresour. Technol.* **2015**, *189*, 177–185. [CrossRef] [PubMed]
50. Yasin, N.H.M.; Mumtaz, T.; Hassan, M.A.; Abd Rahman, N. Food waste and food processing waste for biohydrogen production: A review. *J. Environ. Manag.* **2013**, *130*, 375–385. [CrossRef] [PubMed]
51. Kumar, G.; Mathimani, T.; Rene, E.R.; Pugazhendhi, A. Application of nanotechnology in dark fermentation for enhanced biohydrogen production using inorganic nanoparticles. *Int. J. Hydrogen Energy* **2019**, *44*, 13106–13113. [CrossRef]
52. Mishra, P.; Krishnan, S.; Rana, S.; Singh, L.; Sakinah, M.; Ab Wahid, Z. Outlook of fermentative hydrogen production techniques: An overview of dark, photo and integrated dark-photo fermentative approach to biomass. *Energy Strategy Rev.* **2019**, *24*, 27–37. [CrossRef]
53. Quéméneur, M.; Hamelin, J.; Barakat, A.; Steyer, J.-P.; Carrère, H.; Trably, E. Inhibition of fermentative hydrogen production by lignocellulose-derived compounds in mixed cultures. *Int. J. Hydrogen Energy* **2012**, *37*, 3150–3159. [CrossRef]
54. Ibáñez-López, M.E.; Díaz-Domínguez, E.; Fernández-Morales, F.J.; García-Morales, J.L. Enhancing dark fermentative biohydrogen and VFA production via ozone pre-treatment. *Bioresour. Technol.* **2025**, *419*, 132107. [CrossRef] [PubMed]
55. Zhang, Y.-T.; An, X.; Hao, J.; Dai, X.; Xu, Y. Dual Reinforcement of Biohydrogen Production from Food Waste Dark Fermentation by Thermal–Alkaline Pretreatment Coupled with Nickel-Based Nanoparticles. *Fermentation* **2025**, *11*, 658. [CrossRef]
56. Tenca, A.; Schievano, A.; Perazzolo, F.; Adani, F.; Oberti, R. Biohydrogen from thermophilic co-fermentation of swine manure with fruit and vegetable waste: Maximizing stable production without pH control. *Bioresour. Technol.* **2011**, *102*, 8582–8588. [CrossRef] [PubMed]
57. Yang, G.; Wang, J. Various additives for improving dark fermentative hydrogen production: A review. *Renew. Sustain. Energy Rev.* **2018**, *95*, 130–146. [CrossRef]
58. Wang, J.; Wan, W. Comparison of different pretreatment methods for enriching hydrogen-producing bacteria from digested sludge. *Int. J. Hydrogen Energy* **2008**, *33*, 2934–2941. [CrossRef]
59. European Commission. European Commission. 2021. Available online: https://ec.europa.eu/info/funding-tenders/opportunities/docs/2021-2027/horizon/wp-call/2021-2022/wp-13-general-annexes_horizon-2021-2022_en.pdf (accessed on 22 June 2026).
60. Agapakis, C.M.; Ducat, D.C.; Boyle, P.M.; Wintermute, E.H.; Way, J.C.; Silver, P.A. Insulation of a synthetic hydrogen metabolism circuit in bacteria. *J. Biol. Eng.* **2010**, *4*, 3. [CrossRef] [PubMed]
61. Sekoai, P.T.; Awosusi, A.A.; Yoro, K.O.; Singo, M.; Oloye, O.; Ayeni, A.O.; Bodunrin, M.; Daramola, M.O. Microbial cell immobilization in biohydrogen production: A short overview. *Crit. Rev. Biotechnol.* **2018**, *38*, 157–171. [CrossRef] [PubMed]
62. Show, K.-Y.; Lee, D.-J.; Chang, J.-S. Bioreactor and process design for biohydrogen production. *Bioresour. Technol.* **2011**, *102*, 8524–8533. [CrossRef] [PubMed]
63. Logan, B.; Cheng, S.; Watson, V.; Estadt, G. Graphite Fiber Brush Anodes for Increased Power Production in Air-Cathode Microbial Fuel Cells. *Environ. Sci. Technol.* **2007**, *41*, 3341–3346. [CrossRef] [PubMed]
64. Kausar, A. Nanocomposites of Three-Dimensional Graphene Nanofoams with Polymers—Fundamentals and Progressions. *Polym.-Plast. Technol. Mater.* **2025**, *64*, 253–278. [CrossRef]
65. Gautam, R.; Nayak, J.K.; Ress, N.V.; Steinberger-Wilckens, R.; Ghosh, U.K. Bio-hydrogen production through microbial electrolysis cell: Structural components and influencing factors. *Chem. Eng. J.* **2023**, *455*, 140535. [CrossRef]

66. Hallenbeck, P.C.; Ghosh, D. Advances in fermentative biohydrogen production: The way forward? *Trends Biotechnol.* **2009**, *27*, 287–297. [CrossRef] [PubMed]
67. Thauer, R.K.; Kaster, A.-K.; Seedorf, H.; Buckel, W.; Hedderich, R. Methanogenic archaea: Ecologically relevant differences in energy conservation. *Nat. Rev. Microbiol.* **2008**, *6*, 579–591. [CrossRef] [PubMed]
68. Haji Hassan, U.H. Intensification of Anaerobic Digestion of Food Waste Due to Seeding with CO_2 Microbubbles and Simultaneous Microbubble Stripping to Study Their Role in Alleviating Ammonia Inhibition. Ph.D. Thesis, University of Sheffield, Sheffield, UK, 2023.
69. Kraemer, J.T.; Bagley, D.M. Optimisation and design of nitrogen-sparged fermentative hydrogen production bioreactors. *Int. J. Hydrogen Energy* **2008**, *33*, 6558–6565. [CrossRef]
70. Stams, A.J.M.; Plugge, C.M. Electron transfer in syntrophic communities of anaerobic bacteria and archaea. *Nat. Rev. Microbiol.* **2009**, *7*, 568–577. [CrossRef] [PubMed]
71. Cha, M.; Kim, J.K.; Lee, W.-H.; Song, H.; Lee, T.-G.; Kim, S.-K.; Kim, S.-J. Metabolic engineering of Caldicellulosiruptor bescii for hydrogen production. *Appl. Microbiol. Biotechnol.* **2024**, *108*, 65. [CrossRef] [PubMed]
72. Cha, J.; Choi, Y.; Park, H.; Kim, D.; Baek, G.; Lee, C. Combining pre-fermentation and microbial electrolysis for efficient hydrogen production from food wastewater. *Process Saf. Environ. Prot.* **2024**, *187*, 1471–1480. [CrossRef]
73. Wang, H.; Xu, J.; Sheng, L.; Liu, X.; Lu, Y.; Li, W. A review on bio-hydrogen production technology. *Int. J. Energy Res.* **2018**, *42*, 3442–3453. [CrossRef]
74. Sogani, M.; Maheshwari, K.; Chaturvedi, A.; Sonu, K.; Syed, Z.; Sen, H. Parameters Affecting the Performance of Microbial Electrolysis Cells for Biohydrogen Production. In *Microbial Electrolysis Cells for Biohydrogen Production*; Chae, K.-J., Jadhav, D.A., Pandit, S., Kim, K.-Y., Eds.; Springer Nature: Cham, Switzerland, 2025; pp. 117–137. [CrossRef]
75. Ganguly, A.; Sun, P.; Liu, X.; Delgado, H.E.; Sun, L.; Elgowainy, A. Techno-economic and life cycle analysis of bio-hydrogen production using bio-based waste streams through the integration of dark fermentation and microbial electrolysis. *Green Chem.* **2025**, *27*, 6213–6231. [CrossRef]
76. Zhang, Q.; Jiao, Y.; He, C.; Ruan, R.; Hu, J.; Ren, J.; Toniolo, S.; Jiang, D.; Lu, C.; Li, Y.; et al. Biological fermentation pilot-scale systems and evaluation for commercial viability towards sustainable biohydrogen production. *Nat. Commun.* **2024**, *15*, 4539. [CrossRef] [PubMed]
77. Boshagh, F.; van Niel, E.; Lee, C.-J. Techno-economic and life-cycle analyses of dark fermentative hydrogen production integrated with anaerobic digestion from coffee-manufacturing wastewater under thermophilic and mesophilic conditions. *Bioresour. Technol.* **2025**, *416*, 131737. [CrossRef] [PubMed]
78. Choudhary, M.; Verma, P.; Ray, S. A comprehensive review on bio-electrochemical systems for wastewater treatment: Process, electricity generation and future aspect. *Environ. Dev. Sustain.* **2024**, 1–30. [CrossRef]
79. Marshall, C.W.; Ross, D.E.; Fichot, E.B.; Norman, R.S.; May, H.D. Long-term Operation of Microbial Electrosynthesis Systems Improves Acetate Production by Autotrophic Microbiomes. *Environ. Sci. Technol.* **2013**, *47*, 6023–6029. [CrossRef] [PubMed]
80. Lee, J.-Y.; Sim, Y.-B.; Jung, J.-H.; Pandey, A.K.; Kyung, D.; Kim, S.-H. Greenhouse gas emissions and net energy production of dark fermentation from food waste followed by anaerobic digestion. *Energy* **2024**, *312*, 133559. [CrossRef]
81. Rittmann, S.; Herwig, C. A comprehensive and quantitative review of dark fermentative biohydrogen production. *Microb. Cell Factories* **2012**, *11*, 115. [CrossRef] [PubMed]
82. Rodríguez-Fontalvo, D.; Sánchez, N.; Cobo, M. Sustainable bio-hydrogen production: Assessing economic and environmental implications of a scaled-up industrial bioethanol prototype. *Int. J. Hydrogen Energy* **2024**, *74*, 201–213. [CrossRef]
83. Cavalcante, A.L.G.; Nascimento Dari, D.; Aires, F.I.d.S.; Castro, E.C.d.; Santos, K.M.d.; Santos, J.C.S.d. Advancements in enzyme immobilization on magnetic nanomaterials: Toward sustainable industrial applications. *RSC Adv.* **2024**, *14*, 17946–17988. [CrossRef] [PubMed]
84. Valasara, V.; Ahn, B.; Won, W. Attributional and Consequential Life Cycle Assessments: A Practice-Oriented Framework Integrating System Boundaries and Machine Learning. *J. Chem. Eng. Jpn.* **2026**, *59*, 2662789. [CrossRef]
85. Celestino, É.; Palma-Oliveira, J.M.; Carvalho, A. Innovative roadmap for household organic waste management in the European Union: Pathways to a circular economy. *J. Clean. Prod.* **2025**, *536*, 147153. [CrossRef]
86. OECD. *OECD Environmental Performance Reviews: Belgium 2021, OECD Environmental Performance Reviews*; OECD Publishing: Paris, France, 2021. [CrossRef]
87. Heidrich, E.S.; Dolfing, J.; Scott, K.; Edwards, S.R.; Jones, C.; Curtis, T.P. Production of hydrogen from domestic wastewater in a pilot-scale microbial electrolysis cell. *Appl. Microbiol. Biotechnol.* **2013**, *97*, 6979–6989. [CrossRef] [PubMed]
88. Hallenbeck, P.C. Microbial paths to renewable hydrogen production. *Biofuels* **2011**, *2*, 285–302. [CrossRef]
89. Levin, D.B.; Pitt, L.; Love, M. Biohydrogen production: Prospects and limitations to practical application. *Int. J. Hydrogen Energy* **2004**, *29*, 173–185. [CrossRef]
90. Batstone, D.J.; Keller, J.; Angelidaki, I.; Kalyuzhnyi, S.V.; Pavlostathis, S.G.; Rozzi, A.; Sanders, W.T.M.; Siegrist, H.; Vavilin, V.A. The IWA Anaerobic Digestion Model No 1 (ADM1). *Water Sci. Technol.* **2002**, *45*, 65–73. [CrossRef]

91. Ibrahim, I.; Salehmin, M.N.I.; Balachandran, K.; Hil Me, M.F.; Loh, K.S.; Abu Bakar, M.H.; Jong, B.C.; Lim, S.S. Role of microbial electrosynthesis system in CO_2 capture and conversion: A recent advancement toward cathode development. *Front. Microbiol.* **2023**, *14*, 1192187. [CrossRef] [PubMed]
92. Chen, W.-H.; Biswas, P.P.; Ubando, A.T.; Kwon, E.E.; Lin, K.-Y.A.; Ong, H.C. A review of hydrogen production optimization from the reforming of C1 and C2 alcohols via artificial neural networks. *Fuel* **2023**, *345*, 128243. [CrossRef]
93. Nasr, N.; Hafez, H.; El Naggar, M.H.; Nakhla, G. Application of artificial neural networks for modeling of biohydrogen production. *Int. J. Hydrogen Energy* **2013**, *38*, 3189–3195. [CrossRef]
94. Salamattalab, M.M.; Hasani Zonoozi, M.; Molavi-Arabshahi, M. Innovative approach for predicting biogas production from large-scale anaerobic digester using long-short term memory (LSTM) coupled with genetic algorithm (GA). *Waste Manag.* **2024**, *175*, 30–41. [CrossRef] [PubMed]
95. Mandotra, S.K.; Sharma, C.; Srivastava, N.; Ahluwalia, A.S.; Ramteke, P.W. Current prospects and future developments in algal bio-hydrogen production: A review. *Biomass Conv. Bioref.* **2023**, *13*, 8575–8592. [CrossRef]
96. Nikolaidis, P.; Poullikkas, A. A comparative overview of hydrogen production processes. *Renew. Sustain. Energy Rev.* **2017**, *67*, 597–611. [CrossRef]

Disclaimer/Publisher's Note: The statements, opinions and data contained in all publications are solely those of the individual author(s) and contributor(s) and not of MDPI and/or the editor(s). MDPI and/or the editor(s) disclaim responsibility for any injury to people or property resulting from any ideas, methods, instructions or products referred to in the content.